ELSEVIER

Journal of Alloys and Compounds 446–447 (2007) 166–172

Journal of ALLOYS AND COMPOUNDS

www.elsevier.com/locate/jallcom

Hydrogen storage properties and structure of $La_{1-x}Mg_x(Ni_{1-y}Mn_y)_3$ intermetallics and their hydrides

R.V. Denys [a,b], B. Riabov [a,b], V.A. Yartys [a,*], R.G. Delaplane [c], M. Sato [d]

[a] *Institute for Energy Technology, Kjeller, Norway*
[b] *Physico-Mechanical Institute of the National Academy of Sciences of Ukraine, Lviv, Ukraine*
[c] *The Studsvik Neutron Research Laboratory, Uppsala University, Nyköping, Sweden*
[d] *Department of Applied Science, School of Engineering, Tokai University, Hiratsuka, Kanagawa, Japan*

Received 30 October 2006; received in revised form 22 December 2006; accepted 25 December 2006
Available online 11 January 2007

Abstract

'Hybrid' RNi_3 (R = rare earth metal) crystal structures are built of the slabs of simpler types, $CaCu_5$ and $MgZn_2$. Different affinities of these slabs to hydrogen result in unusual "anisotropic" expansion of the RNi_3 and R_2Ni_7 (R = La, Ce) structures upon hydrogenation. This work focuses on studies of the hydrogenation behaviour of $LaNi_3$ and on the properties of the hydrides of the modified by Mg and Mn La–Ni alloys. The crystal structure of $LaNi_3D_{2.8}$ and the crystal structure and hydrogen storage behaviours of the $La_{1.5}Mg_{0.5}Ni_7$ and $La(Ni_{1-x}Mn_x)_3$ ($x = 0$; 0.067; 0.133; 0.2; 0.267; 0.3; 0.333; 0.4) alloys were in focus. The deuteration of $LaNi_3$ with $PuNi_3$ type of structure leads to the formation of $LaNi_3D_{2.8}$ and is accompanied by a deformation of the metal matrix causing a change of the initial rhombohedral symmetry (space group $R\bar{3}m$) to a monoclinic one (space group $C2/m$; $a = 8.6408(7)$ Å, $b = 4.9281(4)$ Å, $c = 32.774(3)$ Å; $\beta = 90.850(8)^\circ$; $V = 1395.5(2)$ Å^3). Similar to the earlier studied $CeNi_3D_{2.8}$, preferential occupation by deuterium atoms of the AB_2 layers takes place, leading to the "anisotropic" expansion of the unit cell along [0 0 1] ($\Delta c/c = 30.6\%$). 14 occupied D crystallographic sites have 4 chemically different types of metal-atom surroundings, including Ni_4 (2), La_2Ni_2 (2), La_3Ni (6), and La_3Ni_3 (4). Modification of the La–Ni alloys by magnesium and manganese leads to the formation of intermetallic compounds crystallising with the $PuNi_3$, $CeNi_3$, and Ce_2Ni_7-type structures. An ordered substitution of La by Mg in the $MgZn_2$-type slabs was observed, causing a complete alteration of the hydrogenation behaviour of the original $LaNi_3$ alloy. $La_{1.5}Mg_{0.5}Ni_7D_9$ isotropically expands upon its formation and leads to a substantial increase of the stability against hydrogenation-induced amorphisation. On the other hand, replacement of Ni by Mn leads to the change in crystal-structure type from $PuNi_3$ to $CeNi_3$ in the $LaNi_{3-x}Mn_x$ alloys ($x > 0.1$). An ordered substitution of Ni by Mn proceeds inside the RNi_5 slabs only. This decreases the stability of the initial alloy against amorphisation on hydrogenation.

Keywords: Metal hydrides; Gas–solid reactions; Crystal structure; Neutron diffraction

1. Introduction

The hexagonal/trigonal AB_3 and A_2B_7 structures (A – atom of larger size, rare earth metal, Mg; B – atom of smaller size, Ni and Mn) are formed by stacking of AB_5 and A_2B_4 ($2 \times AB_2$) layers of, $CaCu_5$ and $MgZn_2$ types, *r* in different ratios yielding AB_3 ($AB_5 + 2 \times AB_2 = 2 \times AB_3$) and A_2B_7 ($AB_5 + AB_2 = A_2B_7$) stoichiometries. The alteration of the $CaCu_5$ and $MgZn_2$-type slabs proceeds along the [0 0 1] direction and gives either hexagonal $CeNi_3$ and Ce_2Ni_7 types or rhombohedral $PuNi_3$ and Er_2Co_7 structure types.

Hydrogen-absorbing AB_3 intermetallic compounds (A = La, Ce, Y) are known already for more than 30 years [1]. However, increased interest in these AB_3 "hybrid" compounds as hydrogen storage materials has appeared in recent years [2–6], mainly because of the prospects of their electrochemical applications.

The structures of intermetallic hydrides with filled $PuNi_3$-type alloy lattices have been studied for a rather large number of systems such as $HoNi_3H_{1.3–1.8}$ [7,8], $ErNi_3H_{1.2–3.75}$ [9], $ErCo_3H_{4.3}$ [10,11], and YCo_3D_4 [10]. Their hydrogenation is accompanied by different types of lattice expansion, including "anisotropic" enlargement of the unit cell mostly along the [001] direction and relatively modest $\Delta c/c$ values of 7–8%, and

* Corresponding author. Tel.: +47 63 80 64 53; fax: +47 63 81 29 05.
E-mail address: volodymyr.yartys@ife.no (V.A. Yartys).

0925-8388/$ – see front matter © 2007 Elsevier B.V. All rights reserved.
doi:10.1016/j.jallcom.2006.12.137

isotropic expansion, which was observed for $ErNi_3H_{3.75}$ [9]. The crystal structures of the hydrides retained the initial trigonal symmetry of the intermetallic compounds.

On the other hand, a number of "hybrid" compounds during the hydride formation reveal large expansions along the [0 0 1] axis, which reach 25–30% (the basal plane remains almost unchanged). Although this phenomenon has been known for a rather long time [12,13], the structures of such "anisotropic" hydrides have been determined in recent years for only $CeNi_3D_{2.8}$ [14], $La_2Ni_7D_{6.5}$ [15], and $CeY_2Ni_9D_{7.7}$ [16].

The aim of the present work was to study the unusual hydrogenation behaviour of $LaNi_3$, as well as the properties of the hydrogenated and virgin La–Ni alloys modified by Mg and Mn.

The choice of constituents was aimed at replacing the heavier and more expensive La by lighter and cheaper Mg and reaching higher hydrogenation capacities by replacement of Ni by Mn.

2. Experimental

$LaNi_3$ and $LaNi_{3-x}Mn_x$ alloys were prepared by arc-melting mixtures of the corresponding high-purity metals. The 1 at.% excess of La and 2 at.% of Mn were introduced into the alloy in order to compensate for their evaporation during melting. The alloys were sealed in evacuated quartz tubes and annealed for five weeks at 600 °C ($LaNi_3$) or 550 °C (Mn-series). The samples were quenched in ice water after the annealing.

The Mg-substituted material was prepared using the following procedure. A mixture of $LaNi_3$, Mg (with excess of 10 at.%) and Ni powders was compacted into a pellet, wrapped in a Ta foil, and sealed in a quartz tube under 0.5 bar Ar pressure. It was then sintered with the temperature increased in four steps (600, 700, 800, and 980 °C; holding time 4 h at each temperature; heating rate 1 °C/min) and subsequently annealed at 750 °C for 4 days followed with quenching.

Hydrides were synthesised by charging the vacuum-activated (at 300 °C) alloys with H_2 (D_2) gas using two different synthesis routes: (a) a very "mild" synthesis route (small aliquots of D_2 added into an autoclave cooled down to −20 °C) for $LaNi_3$ and Mn-containing samples or (b) constant application of hydrogen synthesis (5 bar H_2(D_2) at room temperature) for the Mg-containing intermetallics.

The prepared alloys and their hydrides have been characterised by means of X-ray diffraction (Siemens D 5000 diffractometer, Cu $K\alpha_1$ radiation, Bragg–Brentano geometry). Powder neutron diffraction (PND) data were collected at the R2 reactor at the Studsvik Neutron Research Laboratory using the high-resolution R2D2 instrument ($\lambda = 1.55134$ Å; 2Θ step 0.05°; 2Θ range 10–120°) [17]. Crystal structure data were derived by Rietveld profile refinements of the XRD and PND data using the GSAS software [18]. Neutron scattering lengths, $b_{La} = 8.24$, $b_{Ni} = 10.30$m, $b_{Mn} = -3.73$, and $b_D = 6.67$ fm, were taken from the GSAS library. The details of the monoclinic distortion of the crystal structure of $LaNi_3D_{2.8}$ deuteride were investigated using high-resolution SR XRD diffraction studies of the deuteride ($\lambda = 0.37504$ Å, at the BM1B instrument, SNBL, ESRF, Grenoble, France).

3. Results

3.1. Intermetallic alloys $LaNi_{3-x}Mn_x$ and $La_{2-x}Mg_xNi_7$

3.1.1. Structure of the $LaNi_3$ alloy

Phase-structural analysis of the prepared $LaNi_3$ material revealed the formation of a single-phase $LaNi_3$ intermetallic compound crystallising with rhombohedral structure and unit cell parameters $a = 5.0817(2)$ and $c = 25.092(1)$ Å [1]. Refinement of the structure indicated the formation of a $PuNi_3$-type structure with the following refined parameters: sp. gr. $R\bar{3}m$ (No. 166); La1 in 3*a*: 0, 0, 0; La2 in 6*c*: 0, 0, 0.1410(1); Ni1 in 3*b*: 0, 0, ½; Ni2 in 6*c*: 0, 0, 0.3327(3); Ni3 in 18*h* 0.500, 0.500, 0.796(2). These data agree well with the reference publication [19].

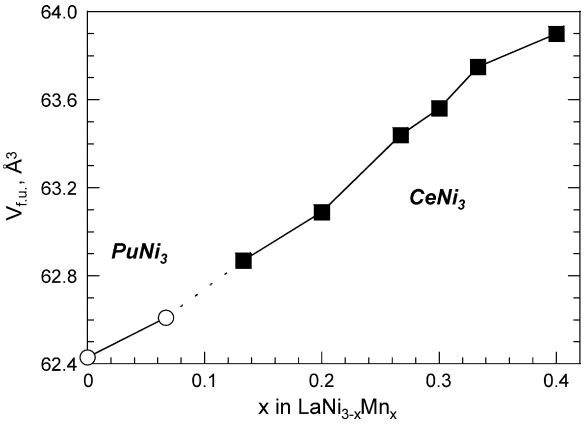

Fig. 1. Increase of the unit cell volumes upon Mn substitution for Ni in the structure of $LaNi_3$ showing area of existence of two types of the structures adopted by the alloys ($PuNi_3$ and $CeNi_3$).

3.1.2. Structure of the $LaNi_{3-x}Mn_x$ alloys

The substitution of smaller Ni atoms by larger Mn atoms results in a monotonic and almost linear increase of the unit cell volumes from 62.4 to 64.0 Å^3 per formula unit (Fig. 1). At a substitution level exceeding $x = 0.1$, the structures of the $LaNi_{3-x}Mn_x$ alloys adopt the hexagonal $CeNi_3$-type structure instead of the rhombohedral $PuNi_3$-type structure characteristic of the initial $LaNi_3$ compound.

In order to study the effect of Mn substitution, the $LaNi_{2.67}Mn_{0.33}$ compound has been investigated by PND (see Fig. 2). From the data presented in Table 1, it can be concluded that Mn substitutes mostly for Ni inside the $CaCu_5$-type layer with a very small amount of Mn replacing Ni atoms in the Kagome nets connecting the AB_5 and AB_2 slabs.

3.1.3. Structure of the $La_{2-x}Mg_xNi_7$

X-ray data indicated that the synthesis process described above did not yield an alloy with AB_3 ($La_{0.67}Mg_{0.33}Ni_3$) composition. A single-phase compound with A_2B_7 ($La_{1.5}Mg_{0.5}Ni_7$)

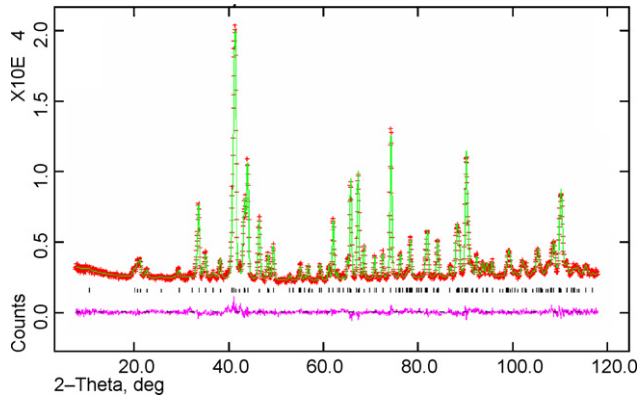

Fig. 2. Powder neutron diffraction pattern of the $LaNi_{2.67}Mn_{0.33}$ alloy (R2D2 instrument, $\lambda = 1.5514$ Å) showing observed (+), calculated (upper line) and difference (lower line) pattern. Positions of the peaks are marked.

Table 1
Crystal structure data for the $LaNi_{2.69}Mn_{0.31}$ alloy (ordered $CeNi_3$ type of structure) refined on the basis of the powder neutron diffraction data

Atom	Site	x	y	z	$U_{iso} \times 100$ (Å^2)	SOF
La1	2*c*	1/3	2/3	1/4	2.1(1)	1.0(−)
La2	4*f*	1/3	2/3	0.4585(2)	1.18(8)	1.0(−)
Ni1	2*a*	0	0	0	0.7(1)	1.0(−)
M2	2*b*	0	0	1/4	1.3(4)	0.472(8)Ni + 0.528(8)Mn
M3	2*d*	1/3	2/3	3/4	1.6(2)	0.728(9)Ni + 0.272(9)Mn
Ni4	12*k*	0.8338(2)	0.6676(4)	0.37166(6)	0.72(4)	0.981(6)Ni + 0.019(6)Mn

Space group $P6_3/mmc$ (No. 194); $a = 5.1404(1)$ Å, $c = 16.7547(6)$ Å; $V = 383.41(2)$ Å^3; composition: $3 \times LaNi_{2.69(2)}Mn_{0.31(2)} = LaNi_{4.14(1)}Mn_{0.86(1)} + 2 \times LaNi_{1.97(1)}Mn_{0.03(1)}$.
$R_p = 0.0300$; $R_{wp} = 0.0376$; $\chi^2 = 1.727$.

Table 2
Crystal structure data for $La_{1.5}Mg_{0.5}Ni_7$ alloy (ordered Ce_2Ni_7 type of structure) refined on the basis of the X-ray diffraction data

Atom	Site	x	y	z	SOF
La1	4*f*	1/3	2/3	0.0209(3)	0.49(1)
Mg1	4*f*	1/3	2/3	0.0209(3)	0.51(1)
La	4*f*	1/3	2/3	0.1728(2)	1.0(−)
Ni1	2*a*	0	0	0	1.0(−)
Ni2	4*e*	0	0	0.1650(4)	1.0(−)
Ni3	4*f*	1/3	2/3	0.8309(5)	1.0(−)
Ni4	6*h*	0.834(1)	0.668(2)	1/4	1.0(−)
Ni5	12*k*	0.8271(7)	0.6542(14)	0.0834(2)	1.0(−)

Space group $P6_3/mmc$ (No. 194); $a = 5.02822(7)$ Å, $c = 24.2032(6)$ Å; $V = 529.95(2)$ Å^3.
$R_p = 0.0284$; $R_{wp} = 0.0371$; $\chi^2 = 1.706$.

stoichiometry was obtained instead. This slight shift in stoichiometry is due to a significant evaporation of Mg during synthesis. Results of the X-ray diffraction data refinements for the $La_{1.5}Mg_{0.5}Ni_7$ alloy are given in Table 2 and Fig. 3. As can be seen from Table 2, magnesium substitutes for La exclusively within the AB_2 slabs of the structure.

3.2. Comparison of the structure of AB_2 and AB_5 slabs in studied intermetallics

Although all three studied intermetallic compounds crystallise with different types of structures, it is nevertheless possible to compare them by analysing the structures of the constituent AB_2 and AB_5 slabs. The relevant crystallographic parameters are provided in Table 3. As can be seen, substitutions of larger La by smaller Mg and smaller Ni by larger Mn have opposite effects on the structures of the intermetallic compounds. As expected, the most significant impact of substitution is observed within the slabs accommodating the "guest" atoms. As compared to the $LaNi_3$ intermetallic, the AB_2 slab shrinks by 9.6% upon substitution of La by Mg; in contrast, the AB_5 slab expands by 4.5% upon substitution of Ni by Mn. The other, "unmodified" slabs vary their parameters very marginally, by less than only 1.2%. Shrinking or expansion of the corresponding slabs of the unit cells leads to the corresponding shortening or elongation of the relevant interatomic distances. The La(Mg)–La(Mg) bonds become 4% shorter than the relevant La–La bonds in the structure of $LaNi_3$. As a result of

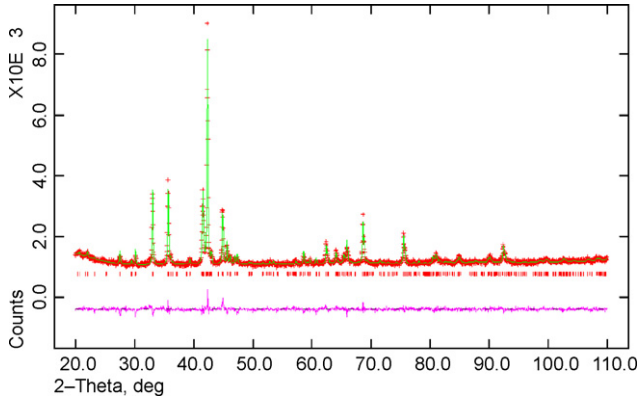

Fig. 3. Powder X-ray diffraction pattern of the $La_{1.5}Mg_{0.5}Ni_7$ alloy showing observed (+), calculated (line) and difference (lower line) pattern. Positions of the peaks are marked.

Table 3
Selected crystallographic parameters of the AB_2 and AB_5 slabs in the crystal structures of $LaNi_3$, $LaNi_{2.69}Mn_{0.31}$, and $La_{1.5}Mg_{0.5}Ni_7$

Compound	$LaNi_3$	$LaNi_{2.69}Mn_{0.31}$	$La_{1.5}Mg_{0.5}Ni_7$
Str. type	$PuNi_3$	$CeNi_3$	Ce_2Ni_7
a (Å)	5.0817(2)	5.1404(1)	5.02822(7)
$\Delta a/a_{LaNi_3}$	–	1.2%	−1.1%
c (Å)	25.092(1)	16.7547(6)	24.2032(6)
Data source	XRD	PND	XRD
AB_2 layer			
Composition	$2 \times LaNi_2$	$2 \times LaNi_{1.97}Mn_{0.03}$	$2 \times La_{0.5}Mg_{0.5}Ni_2$
c_{AB_2}	4.371	4.299	4.037
$\Delta c_{AB_2}/c_{AB_2}$	–	−1.6%	−7.6%
c/a	0.86	0.84	0.80
V	97.8	98.4	88.4
$\Delta V_{AB_2}/V_{AB_2}$	–	0.6%	−9.6%
La(Mg)–La(Mg)	3.204	3.277	3.074
La(Mg)–Ni	3.004–3.186	3.048–3.211	2.885–2.947
Ni–Ni	2.541–2.632	2.578–2.610	2.420–2.518
AB_5 layer			
Composition	$LaNi_5$	$LaNi_{4.14}Mn_{0.86}$	$LaNi_5$
c_{AB_5}	3.993	4.077	4.032
$\Delta c_{AB_5}/c_{AB_5}$	–	2.1%	1.0%
c/a	0.79	0.79	0.80
V	89.3	93.3	88.3
$\Delta V_{AB_5}/V_{AB_5}$	–	4.5%	−1.1%
La–Ni(Mn)	2.934–3.232	2.968–3.280	2.904–3.317
Ni(Mn)–Ni(Mn)	2.541–2.632	2.519–2.524	2.420–2.905
V_{AB_2}/V_{AB_5}	1.09	1.05	1.00

shrinking of the AB_2 slab in the Mg-substituted material, the volumes of the AB_2 and AB_5 slabs become equal (Table 3).

3.3. Hydrogenation properties

Only very low synthesis temperatures and starting pressures of hydrogenation allowed us to synthesise the crystalline $LaNi_3D_{2.8}$. Deuterium was introduced step-by-step in small portions starting from 0.01 to 0.05 bar D_2, in about 20 steps, before reaching a final pressure of 1 bar. This yielded a deuteride with the stoichiometry $LaNiD_{\sim 3}$. The hydrogenation of $LaNi_3$ by immediate injection of 1 bar D_2 into the autoclave resulted in almost complete amorphisation of the material, because of the high reaction rate and high heat of hydrogenation causing the temperature increase. For the Mn-substituted alloys the amorphisation occurred even at −20 °C. The volumetrically measured capacity of these amorphous hydrides were found to be approximately the same as those reported for $LaNi_3$ [4]: $LaNi_{2.8}Mn_{0.2}D_{4.3}$ and $LaNi_{2.6}Mn_{0.4}D_{4.5}$.

On the other hand, the magnesium compound was deuterated using a synthesis pressure of 5 bar D_2 with saturation reached in just 15 min. The synthesis led to a formation of crystalline $La_{1.5}Mg_{0.5}Ni_7D_9$. It is formed via an isotropic expansion of the unit cell ($\Delta a/a = 7.1\%$, $\Delta c/c = 9.3\%$, $\Delta V/V = 25.3\%$) [20]. The structural data for the deuteride $La_{1.5}Mg_{0.5}Ni_7D_9$ will be published elsewhere [20].

3.4. Crystal structure of the $LaNi_3D_{2.8}$ deuteride

The X-ray diffraction study of $LaNi_3D_{2.8}$ showed a pronounced linear expansion of the original trigonal unit cell along [0 0 1], $\Delta c/c = 27.8\%$ together with a slight contraction in the basal plane, $\Delta a/a \sim -2.5\%$. From the analysis of the synchrotron X-ray diffraction pattern, the splitting of the $h\,k\,l$, $h\,h\,l$, and $h\,k\,0$ peaks was evident with the $0\,0\,l$ reflections remaining unsplit (see inset in Fig. 4 as illustration). Thus, lowering of the symmetry of the original trigonal structure was concluded. From group–subgroup relations, the following transformation of the original trigonal unit cell into the monoclinic one for the hydride was deduced: $R\bar{3}m \rightarrow P\bar{3}m1 \rightarrow C2/m$ ($a_{mon} = (a + 2b)_{trig}$; $b_{mon} = -a_{trig}$; $C_{mon} = C_{trig}$; $V_{mon} = 2\ V_{trig}$). The monoclinic deformation of the structure was further confirmed by analysis of the PND profiles. Besides the broadening of the pattern due to the splitting of the peaks, extra peaks appeared in the diffraction profile in addition to those allowed by the trigonal symmetry; the most distinct of these peaks are marked in Fig. 4.

The refinement of the XRD data revealed a strong expansion of the AB_2 layers of the structure with the AB_5 layers remaining unchanged. This feature makes the structure of the monoclinically deformed $LaNi_3D_{2.8}$ deuteride similar to the previously studied, chemically related, "anisotropic", orthorhombic $CeNi_3D_{2.76}$ [14] and hexagonal $La_2Ni_7D_{6.1}$ [15] deuterides.

Starting from the known structure of the metal sublattice, obtained from a transformation from the trigonal unit cell to the monoclinic expanded one, the deuterium atoms were located using the difference Fourier synthesis process. Several steps of such a process were applied before all 14 D sites were located. All deuterium atoms in $LaNi_3D_{2.8}$ are located inside the $MgZn_2$-type layers or on the borders between the AB_5 and AB_2 slabs (D7 and D8 sites in the Table 4) with no D atoms inside the AB_5 slabs.

The results of the Rietveld refinements of PND data are presented in Table 4. The crystal structures of the initial intermetallic $LaNi_3$ compound and corresponding $LaNi_3D_{2.8}$ deuteride are shown in Fig. 5.

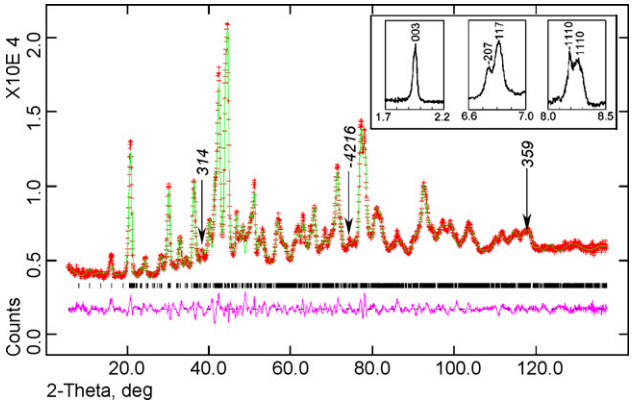

Fig. 4. Powder neutron diffraction pattern of the $LaNi_3D_{2.8}$ deuteride showing calculated (upper line), observed (+) and difference (lower line) pattern. Positions of the peaks are marked. Arrows indicate peaks, which are not allowed in the trigonal symmetry. Inlets show splitting of the peaks in the SR XRD pattern because of a monoclinic distortion of the metal matrix of the deuteride.

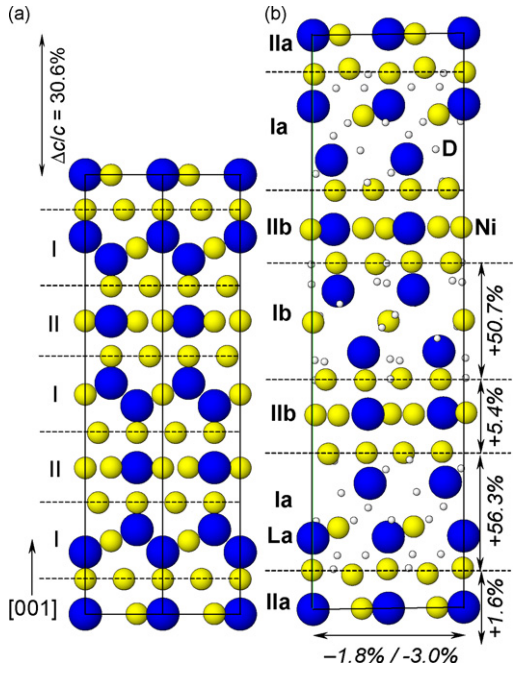

Fig. 5. Crystal structures of the $LaNi_3$ intermetallic compound (a) and the $LaNi_3D_{2.8}$ deuteride, (b) "anisotropic" expansion of the metal sublattice upon hydride formation is shown for two different types of the available structure slabs (I –$MgZn_2$ and II –$CaCu_5$). Due to monoclinic distortion, the AB_2 slabs in the structure of hydride become nonequivalent, having $LaNi_2D_{4.5}$ (I*a*) and $LaNi_2D_{3.2}$ (I*b*) compositions. Difference in deuterium content between the AB_5 layers (II*a* and II*b*) is less pronounced, $LaNi_5D_{0.25–0.28}$.

Table 4
Crystal structure data for $LaNi_3D_{2.8}$

Atom	Site	x/y[a]	z	Fraction		Occupied interstice[b] (corresponding site in the IMC)
La1	2*a*	0	0	1.0(−)		(La1)
La2	4*i*	0.636(2)	0.3387(6)	1.0(−)		
La3	4*i*	0.002(3)	0.8760(6)	1.0(−)		(La2)
La4	4*i*	0.378(2)	0.7823(6)	1.0(−)		
La5	4*i*	0.665(3)	0.4461(7)	1.0(−)		
Ni1	2*c*	0	½	1.0(−)		(Ni1)
Ni2	4*i*	0.667(2)	0.8586(5)	1.0(−)		
Ni3	4*i*	0.016(2)	0.6615(4)	1.0(−)		(Ni2)
Ni4	4*i*	0.676(3)	0.0002(6)	1.0(−)		
Ni5	4*i*	0.668(2)	0.6627(5)	1.0(−)		
Ni6	4*i*	0.493(2)	0.9319(6)	1.0(−)		(Ni3)
Ni7	8*j*	0.740(1)/0.749(3)	0.0592(3)	1.0(−)		
Ni8	4*i*	0.855(2)	0.7288(6)	1.0(−)		
Ni9	8*j*	0.899(2)/0.262(3)	0.2704(4)	1.0(−)		
Ni10	4*i*	0.154(2)	0.3972(6)	1.0(−)		
Ni11	8*j*	0.916(2)/0.261(3)	0.3999(4)	1.0(−)		
Layer I*a*						
D1	4*i*	0.4930(2)	0.1587(1)	1.0(−)	La_3Ni *c*	
D2	4*i*	0.134(3)	0.1804(4)	1.0(−)	La_3Ni *c*	
D3	4*i*	0.334(2)	0.1965(8)	1.0(−)	La_3Ni *c*	
D4	8*j*	0.240(2)/0.249(2)	0.1518(6)	1.0(−)	La_3Ni *c*	
D5	4*i*	0.8979(4)	0.06109(4)	0.57(7)	La_2Ni_2 *a*	
D6	4*i*	0.650(2)	0.092(1)	1.0(−)	La_3Ni_3 *d*	
D7	4*i*	0.017(3)	0.2387(9)	1.0(−)	La_3Ni_3 *d*	
D8	4*i*	0.326(7)	0.249(2)	0.75(4)	La_3Ni_3 *e*	
D9	4*i*	0.331(5)	0.09566(4)	1.0(−)	Ni_4 *b*	
Layer I*b*						
D10	4*i*	0.138(2)	0.4727(8)	0.70(7)	La_3Ni *c*	
D11	8*j*	0.435(5)/0.218(4)	0.5026(4)	0.5(−)	La_3Ni *c*	
D12	4*i*	0.5126(2)	0.39418(5)	0.25(6)	La_2Ni_2 *a*	
D13	4*i*	0.406(9)	0.4275(3)	0.54(5)	La_3Ni_3 *d*	
D14	4*i*	0.001(5)	0.4727(7)	0.80(4)	Ni_4 *b*	

Space group *C*2/*m* (No. 12): $a = 8.6392(2)$ Å; $b = 4.9265(5)$ Å; $c = 32.780(4)$ Å; $\beta = 90.85(1)^\circ$; $V = 1395.8(2)$ Å^3. U_{iso} was constrained to be equal for the chemically similar types of the atoms: La1–La2 (0.5(3)), La3–La5 (1.3(2)); Ni1–Ni2 (3.6(5)); Ni3–Ni5 (1.1(1)); Ni6–Ni11 (0.75(7)); D1–D14 (2.2(2) Å$^2 \times 10^{-2}$); $R_{wp} = 0.0397$; $R_p = 0.0310$.

[a] $y = 0$ if the other values are not stated.

[b] Letter after the type of interstice corresponds to the labeling in the Fig. 6.

4. Discussion

The study of the substitution of the constituent atoms in the structure of $LaNi_3$ by Mg and Mn revealed that it selectively proceeds in the different layers of the structure:

- In $La_{0.75}Mg_{0.25}Ni_{3.5}$ Mg substitutes for 50% of La within the Laves-type AB_2 slabs only: ($LaNi_2 \rightarrow La_{0.5}Mg_{0.5}Ni_2$). The AB_5 slab remains unchanged and has the $LaNi_5$ composition.
- An opposite behaviour is observed when Ni is substituted by Mn in $LaNi_3$ forming $LaNi_{2.69}Mn_{0.31}$: $LaNi_2$ slabs remain nonmodified while the Ni substitution by Mn proceeds inside the AB_5-type slabs until reaching the stoichiometry $LaNi_{4.14}Mn_{0.86}$. Such a substitution reveals an opposite trend to those observed in the structures of the AB_5 $LaNi_{4.1}Mn_{0.91}$ intermetallic, where Mn atoms mostly substitute for Ni atoms within the Kagome nets [21]. The unit cell of the latter AB_5 phase has smaller volume (91.6 Å^3 compared to 93.3 Å^3 for the AB_5 layer in $LaNi_{2.69}Mn_{0.31}$ (Table 4)).
- Substitution of Ni by Mn proceeds until reaching a Mn content of at least 0.4 at. Mn/f.u. Increase of the Mn content above 0.1 at. Mn/AB_3 leads to the change of the structure type from trigonal $PuNi_3$ to hexagonal $CeNi_3$. The substitution is accompanied by an approximately linear increase in the unit cell volumes with the rise in Mn content from 62.4 up to 63.9 Å^3/f.u. AB_3.

Similar ways of both types of substitution were observed in [22] during the synthesis of the hexagonal $La_4Mg(Ni,Co)_{19}$ (Pr_5Co_{19} structure type), where the 3d-element, cobalt, substitutes for Ni in the AB_5 layers only and Mg replaces La atoms exclusively in the AB_2 layer.

The hydrogenation of the $LaNi_3$ under mild conditions resulted in the synthesis of the $LaNi_3D_{2.8}$, whose formation is

accompanied by the monoclinic distortion of the metal matrix and leads to the insertion of the D atoms only into the AB_2 slabs of structure. This leads to a large elongation of the unit cell along the [0 0 1] direction by 30.6%, the AB_2 layers being expanded by 50.7–56.3%. The basal plane of the unit cell contracts during the hydride formation by −1.8/−3.0%. Such features of the $LaNi_3D_{2.8}$ deuteride structure are common to the other known structures of the "anisotropic" hydrides [14–16].

Monoclinic distortion of the unit cell reveals differences in the expansion of the metal sublattice caused by variations of H content of the initially equivalent in the trigonal structure layers of the AB_2 or AB_5 types. This distortion results in formation of stronger (I*a*: AB_2; II*b*: AB_5) and weaker (I*b*: AB_2; II*a*: AB_5) expanded layers, where a more pronounced expansion agrees well with higher hydrogen content in the corresponding AB_2-type I*a* layer–$LaNi_2D_{4.52}$ ($\Delta c/c = 56.3\%$) compared to the I*b* layer with lower D content, $LaNi_2D_{3.17}$, and smaller linear expansion, $\Delta c/c = 50.7\%$ (Fig. 5). Coordination numbers of La atoms in LaDx polyhedra withing the I*a* layer are 12 and 9. These coordination characteristics are similar to those observed in the crystal structure of $CeNi_3D_{2.8}$ (12 and 7 D atoms for Ce atoms) [14]. In case of the I*b* layer, formation of disordered LaD_{11} polyhedra takes place.

In the structure of $LaNi_3D_{2.8}$, hydrogen atoms occupy 14 types of interstices with 5 different types of surroundings (Fig. 6). These include 4 types already existing in the structure of $LaNi_3$ intermetallic alloy interstices (two types of La_2Ni_2 and two types of Ni_4 tetrahedra Fig. 6a–b) and ten new types of sites formed due to the distortion of the metal matrix within the AB_2 slab (Fig. 6c–e). The latter include 4 La_3Ni_3 and 6 La_3Ni interstices. These new types of sites are similar to those filled by H atoms in the "anisotropic" structures of $CeNi_3D_{2.8}$ [14] and $La_2Ni_7D_{6.5}$ [15].

We note that D3 and D8 atoms occupy neighbouring interstices with a common La_3 triangular face (upper and lower parts of the cluster shown in Fig. 6e. This results in a D3–D8 separation of 1.74 Å. Such a feature is similar to that observed for the hexagonal $RNiInD_{1.33-x}$ deuterides with short D. . .D distances (1.56–1.63 Å) formed because of a double filling by D atoms of the trigonal bipyramids R_3Ni_2 [23].

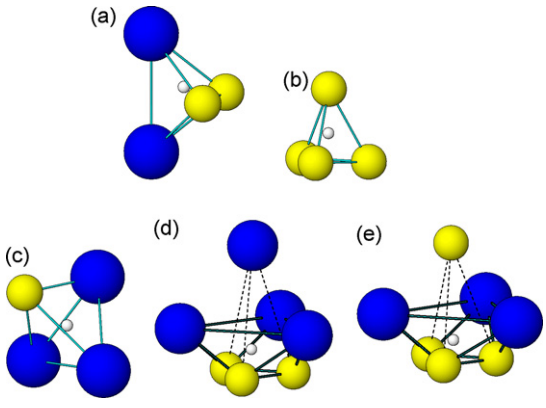

Fig. 6. Types of occupied interstices in the structure of $LaNi_3D_{2.8}$, both existing in the $LaNi_3$ structure (a, b) and, also, formed due to the deformation of the AB_2 layers (c–e).

The shortest interatomic distances observed in the structure of $LaNi_3D_{2.8}$ are: La–La 3.58 Å, La–Ni 2.67 Å, Ni–Ni 2.38 Å (within a contracted $LaNi_5$-layer), La–D 2.16 Å, Ni–D 1.47 Å, and D–D 1.74 Å. All other D–D distances except D3–D8 exceed 1.8 Å. The D sites distanced at 1.44 (D12–D13) and 1.13 Å (D11–D11), are never simultaneously occupied since their occupation numbers are low.

Maximum hydrogen capacity for the considered model of the deuterium sublattice corresponds to $LaNi_3D_{3.11}$. This means that at higher hydrogen content exceeding 3.11 at. H/$LaNi_3$, hydrogen atoms should also occupy the AB_5 slabs.

The formed crystalline $LaNi_3D_{2.8}$ deuteride has a much lower hydrogen storage capacity compared to the maximum capacity observed for the completely amorphous $LaNi_3H_{4.5}$ [4] which indicates that on amorphisation, the structure of the metal sublattice changes.

As it follows from the data of the Table 4 and Fig. 5, in the structure of the $LaNi_5D_{2.8}$ deuteride ~ 90% of deuterium atoms are located within the AB_2 slabs, and 10% are situated on the boundaries between the AB_2 and AB_5 slabs (sites D7–D8 in the Table 3). Such a distribution corresponds to the alternation of the $LaNi_2D_{3.17–4.52}$ and $LaNi_5D_{0.25–0.28}$ layers. Hydrogen contents of the AB_2 layers for both $LaNi_3D_{2.8}$ and $CeNi_3D_{2.76}$ are rather similar (4.0 and 3.0 at. H/f.u. in both cases). These values are also close to the hydrogen storage capacity of the amorphous Laves-type $LaNi_2$-based hydride $LaNi_2H_{>3.5}$ [24]. However, in the hybrid "anisotropic" structures, the hydrogenated AB_2 layer remains crystalline, possibly because of a stabilising effect of the nonhydrogen-absorbing AB_5 slabs. When the AB_5 slabs become expanded, the crystallinity of the hybrid hydride structure worsens before vanishing. The $LaNi_3D_{2.8}$ in this relation is less stable compared to the $CeNi_3D_{2.8}$, since the pressures of hydrogen uptake by the AB_5 phases $LaNi_5$ and $CeNi_5$ are 2 and 48 bar, respectively [14]. Since they are significantly lower for $LaNi_5$, this makes its hydrogenation inside the AB_3 alloy much more easily achievable.

Ni substitution by Mn in the structure of $LaNi_5$ is known to reduce the hydride formation pressures [21]. Increase of Mn content leads to the expansion of the AB_5^- slabs in the Mn-containing samples; thus, hydrogenation pressures for the AB_5 slabs should be at lower pressures compared to $LaNi_3$. Such easier hydrogenation, furthermore, explains why these alloys appear to be less stable against the hydrogen-induced amorphisation. This difference in hydrogen affinity of the different slabs of the structure can be concluded from the analysis of the structures of the initial intermetallics. As long as the volume of the AB_2 slab is larger than that of the AB_5 slab, the AB_2 slabs remain more active with respect to hydrogenation and, thus, the formation of the "anisotropic" hydrides can be expected. When the volumes of slabs in the initial compound become equal because of expansion of the AB_5 slabs caused by the doping elements (Mn), this reduces differences in the hydrogenation affinities of the AB_5 and AB_2 slabs. Similar H uptake by both layers causes alteration of the hydrogenation behaviour from an "anisotropic" (H in the AB_2 layers and no H uptake by the AB_5 layer) to an "isotropic" hydride with even distribution of the H atoms between these two types of slabs. Such changes can be reached

by a selective substitution of the constituent atoms within the AB_2 layer of the initial AB_3 intermetallic phase. The examples of such substitution are La replacement by Mg (this work) or Y in the structure of $LaY_2Ni_9D_{12.8}$ [16].

5. Conclusions

'Hybrid' crystal structures of the La–Ni intermetallics formed by the stacking of the AB_2 (Laves phase) and AB_5 ($CaCu_5$) type slabs were selectively modified by a partial substitution of La by Mg and of Ni by Mn. Mg atoms enter the AB_2 slabs only, whereas Mn atoms mostly replace Ni atoms inside the AB_5^- slab, with just small amounts of Mn observed in the network joining the AB_5 and AB_2 slabs.

Because of the thermodynamically metastable character of the hydride formed, $LaNi_3$ easily becomes amorphous on hydrogenation. Its crystalline hydride was synthesised only during the synthesis at −20 °C and by using low hydrogenation pressures, below 1 bar. Mg increases the stability of the metal sublattice towards its disproportionation in hydrogen: the crystalline hydride was obtained at room temperature and a hydrogen charging pressure of 5 bar. In contrast, Mn reduces stability of the intermetallic alloy; only amorphous hydrides were obtained even when proceeding with synthesis of the hydride at subzero temperatures and at reduced H_2 pressures.

Upon hydrogenation, the rhombohedral $LaNi_3$ forms a monoclinically distorted $LaNi_3D_{2.8}$ deuteride. Hydrogen atoms occupy only AB_2 slabs in the structure. They fill interstices both existing in the original $LaNi_3$ and formed because of the H-induced deformation of the metal matrix. Such selective filling by H of the metal sublattice results in a very pronounced expansion of the AB_2 slabs and of the unit cells in total along the [0 0 1] direction (50.7–56.3% and 30.6%, respectively). Deuterium atoms occupy 14 different types of interstices with 4 different types of surroundings, La_2Ni_2, Ni_4 (both present already in the initial intermetallics), La_3Ni and La_3Ni_3 interstices (formed because of substantial shifts of the atoms within the AB_2 slabs). La atoms in the AB_2 slabs are surrounded by 12, 11, or 9 hydrogen atoms.

Acknowledgements

This work was supported by the Nordic Energy Research (Project 46-02 NORSTORE) and NEDO, Japan (Project "Novel Intermetallic Hydrides with High Volume Density and Advanced Surface Properties" between IFE and Tokai University).

References

[1] K.H.J. Buschow, H.H. van Mal, J. Less-Common Met. 29 (2) (1972) 203–210.
[2] R. Baddour-Hadjean, L. Meyer, J.P. Pereira-Ramos, M. Latroche, A. Percheron-Guégan, Electrochim. Acta 46 (15) (2001) 2385–2393.
[3] B. Liao, Y.Q. Lei, L.X. Chen, G.L. Lu, H.G. Pan, Q.D. Wang, J. Alloys Compd. 376 (2004) 186–195.
[4] J. Chen, H.T. Takeshita, H. Tanaka, N. Kuriyama, T. Sakai, I. Uehara, M. Haruta, J. Alloys Compd. 302 (2000) 304–313.
[5] K. Kadir, T. Sakai, I. Uehara, J. Alloys Compd. 302 (2000) 112–117.
[6] K. Kadir, T. Sakai, I. Uehara, J. Alloys Compd. 257 (1997) 115–121.
[7] S.P. Solov'ev, N.V. Fadeeva, V.A. Yartys, V.V. Burnasheva, K.N. Semenenko, Sov. Solid State Phys. 23 (1981) 1226 (in Russian).
[8] Y.E. Filinchuk, D. Sheptyakov, K. Yvon, J. Alloys Compd. 413 (2005) 106–113.
[9] Y.E. Filinchuk, K. Yvon, J. Alloys Compd. 404–406 (2005) 89–94.
[10] M.I. Bartashevich, A.N. Pirogov, V.I. Voronin, T. Goto, M. Yamaguchi, I. Yamamoto, J. Alloys Compd. 231 (1995) 104–107.
[11] Y.E. Filinchuk, K. Yvon, J. Solid State Chem. 179 (2006) 1041–1052.
[12] V.A. Yartys, V.V. Burnasheva, K.N. Semenenko, N.V. Fadeeva, S.P. Solov'ev, Int. J. Hydrogen Energy 7 (12) (1982) 957–965.
[13] R.H. Van Essen, K.H.J. Buschow, J. Less-Common Met. 70 (2) (1980) 189–198.
[14] V.A. Yartys, O. Isnard, A.B. Riabov, L.G. Akselrud, J. Alloys Compd. 356–357 (2003) 109–113.
[15] V.A. Yartys, A.B. Riabov, R.V. Denys, M. Sato, R.G. Delaplane, J. Alloys Compd. 408–412 (2006) 273–279.
[16] M. Latroche, V. Paul-Boncour, A. Percheron-Guégan, J. Solid State Chem. 177 (2004) 2542–2549.
[17] A. Wannberg, M. Gronros, A. Mellergard, L.-E. Karlsson, R.G. Delaplane, B. Lebech, Z. Kristallogr. Suppl. 23 (2006) 195.
[18] A.C. Larson, R.B. von Dreele, General Structure Analysis System, LANL, 1994.
[19] A.V. Virkar, A. Raman, J. Less-Common Met. 18 (1969) 59–66.
[20] R.V. Denys, V.A. Yartys, R.G. Delaplane, Unpublished results.
[21] C. Lartigue, A. Percheron-Guégan, J.C. Achard, F. Tasset, J. Less-Common Met. 75 (1) (1980) 23–29.
[22] E. Akiba, H. Hayakawa, T. Kohno, J. Alloys Compd. 408–412 (2006) 280–283.
[23] V.A. Yartys, R.V. Denys, B.C. Hauback, H. Fjellvåg, I.I. Bulyk, A.B. Riabov, Ya.M. Kalychak, J. Alloys Compd. 330–332 (2002) 132–140.
[24] V. Paul-Boncour, A. Percheron-Guégan, N. Diaf, J.C. Achard, J. Less-Common Met. 131 (1–2) (1987) 201–208.